

M. A. Kazemi-Lari · S. A. Fazelzadeh

Flexural-torsional flutter analysis of a deep cantilever beam subjected to a partially distributed lateral force

Received: 7 July 2014 / Revised: 6 October 2014 / Published online: 21 November 2014
© Springer-Verlag Wien 2014

Abstract The non-conservative instability of a deep cantilever beam subjected to a lateral force with partial distribution has been verified. The governing equations have been derived using the extended Hamilton's principle, and the Galerkin method has been implemented to approximate the response of system. The influence of system parameters like mass centroid offset, radius of gyration, fundamental frequencies ratio, load distribution model, and the added effect of a free stream with chord-wise velocity has been examined on the instability boundaries of the beam. In addition, the validity of the proposed model has been corroborated in comparison with the available results in the literature.

List of symbols

A	Beam cross sectional area
b	Beam semi-width
c	Mass centroid offset from elastic axis
E	Young's modulus
G	Shear modulus
$H(x)$	Heaviside step function
$I_{y'}$	Beam's moment of inertia from y' axis
$I_{z'}$	Beam's moment of inertia from z' axis
J	Torsional rigidity
$\mathbf{i}, \mathbf{j}, \mathbf{k}$	Unit vectors associated with undeformed beam coordinate system
$\mathbf{i}', \mathbf{j}', \mathbf{k}'$	Unit vectors associated with deformed beam coordinate system
k_m	Radius of gyration
l	Beam length
$M_{z'}$	Bending moment about the z' axis
\bar{p}	Intensity of the distributed follower force
t	Time
T	Kinetic energy
u, v, w	Displacements in the x, y, z directions, respectively
U	Strain energy
U_∞	Free stream velocity

M. A. Kazemi-Lari · S. A. Fazelzadeh (✉)
School of Mechanical Engineering, Shiraz University, 71348-51154 Shiraz, Iran
E-mail: fazelzad@shirazu.ac.ir
Tel.: +98 7116133238

M. A. Kazemi-Lari
E-mail: kazemilari@shirazu.ac.ir

x, y, z	Mutually perpendicular axis system with x along the undeformed beam
$\delta(\)$	Variational operator
δW	Virtual work of the non-conservative forces
$\varepsilon_{xx} \ \varepsilon_{xy} \ \varepsilon_{xz}$	Engineering strains
$\sigma_{xx} \ \sigma_{xy} \ \sigma_{xz}$	Engineering stresses
ω_θ	Fundamental torsion frequency
ρ_∞	Free stream density
ρ	Beam density
θ	Twist about elastic axis
$\kappa_{z'}$	Bending curvature about the z' axis
$(\)'$	Derivative with respect to x
$(\)$	Derivative with respect to t

1 Introduction

Follower forces have been a matter of research for more than 60 years owing to their real nature, numerous practical applications, and being a possible catastrophic failure source. Also, they have been a matter of interest because of the non-conservative features and the distinctive response of systems subjected to these kinds of forces. Different patterns of follower forces are tangential [1] and lateral [2], as well as concentrated [3] and distributed [4]. A broad investigation on types and characteristics of follower forces has been carried out by Bolotin [5], Simitzes and Hodges [6], and Langthjem and Sugiyama [7].

Cantilevered beams might be subjected to lateral follower forces in different examples such as the influence of an end thrust applied on aircraft wing [8], powered engines in the middle portion of a wing [9], applied loads on an aircraft wing as a result of actuated high lift devices, ailerons, or spoilers during flight, friction-induced problems, and in steel and offshore structures.

The problem of non-conservative instability of a cantilever under the influence of a lateral force has been first studied by Como [2]. The lateral load was considered as a follower force at the tip of the cantilever that was modeled as the effect of a jet engine. The jet engine was modeled as a lumped mass attached to the cantilever, and the effect of the cantilever mass was ignored in the equations of motion. The critical follower force was found for this simplified case via the approximation methods. Later, Feldt and Herrmann [10] investigated the bending-torsional flutter of a cantilevered wing subjected to an end lateral follower force. Moreover, the effects of a lumped mass at the end and the aerodynamic loadings with Theodorsen model were studied. The destabilizing influence of the follower force and the stabilizing effect of the end mass were proved. Also, it was shown that the structural damping might have pronounced influence on the dynamic instability of the wing.

Bending-torsion flutter of deep cantilever beams subjected to an end thrust with and without the presence of aerodynamic loadings has been investigated by Hodges [8] and Hodges et al. [11]. Changes in the critical follower force versus the physical parameters of the system like mass centroid offset, radius of gyration, ratio of flexural to torsional rigidities, and the velocity of chord-wise flow were examined. Fazelzadeh et al. [9] studied the torsional-flexural aeroelastic instability characteristics of aircraft wings with arbitrary located lumped mass under the influence of a concentrated follower force. The lumped mass was modeled as an aircraft engine with mass centroid offset in three directions. The influence of the chord-wise and span-wise locations of the mass and the magnitude of the follower force on the flutter speed and frequency of the aircraft wing was studied. In addition, the effect of a time-dependent lateral follower force modeled as an engine thrust and the added effect of aerodynamic loadings on the dynamic instability of aircraft wings were analyzed by Mazidi et al. [12]. The stabilizing and destabilizing influence of the follower force with respect to its chord-wise and span-wise location was examined. Furthermore, the complete nonlinear aeroelastic trim and stability analysis of a flying wing aircraft considering the effect of four powered engines attached on the wings were studied by Mardanpour et al. [13] and the flutter speed and frequencies were derived for various placements of engines.

The dynamic instability of cantilever beams under the influence of a partially distributed tangential force was explored by Fazelzadeh and Kazemi-Lari [14], and the stable regions were derived for different load distribution models. Also, the effects of an arbitrary located lumped mass and an elastic foundation were investigated on the dynamic instability boundaries. Moreover, Fazelzadeh and Kazemi-Lari [15] studied the flutter and divergence of deep cantilever beams subjected to a laterally distributed follower force. The influences of bending to torsion frequency ratio, beam's radius of gyration, and mass centroid offset on the static and dynamic critical forces were analyzed.

The present study investigates the bending-torsion instability of a deep cantilever beam subjected to a partially distributed lateral follower force under the influence of a free stream. The changes in the beam’s mass centroid offset, radius of gyration, and flexural and torsional rigidities which considerably affect the type and magnitude of the critical follower force on the stability boundaries of the system are examined. Also, different patterns are analyzed for the distribution of the follower force along the beam’s span. Moreover, the influence of free stream velocity and the resulting lift and moment exerted on the beam on the instability characteristics are studied. In addition, in order to verify the validity of the current formulations, the simulation results are compared with available results in the literature.

2 Mathematical modeling

2.1 Problem description

The isotropic deep cantilever beam of uniform cross section is demonstrated in Fig. 1. A partially distributed follower force with constant magnitude of \bar{p} is laterally exerted on the beam. In addition, the beam is subjected to a free stream with a uniform chord-wise flow velocity of U_∞ . The distribution of area cross section is such that the value of flexural rigidity in the z direction is much greater than its value in the y direction, i.e., $EI_z \gg EI_y$. Also, the negligible effects of rotatory inertia and deformations due to the transverse shear force in bending analysis, as well as warping in torsion analysis, are not considered to avoid inessential complexity in the governing equations [8, 16].

2.2 Problem formulation

To establish the governing equations, the extended Hamilton’s principle is used as below:

$$\delta \int_{t_1}^{t_2} (T - U) dt + \int_{t_1}^{t_2} \delta W = 0, \tag{1}$$

where the first variation of the kinetic energy can be readily written as [8]

$$\delta T = \int_0^l -\rho A [\dot{v}\delta v + \dot{w}\delta w + c\ddot{\theta}\delta\theta + k_m^2\ddot{\theta}\delta\theta + c\dot{w}\delta\theta] dx. \tag{2}$$

Also, the beam’s strain energy can be generally described as

$$U = \frac{1}{2} \int_0^l \int \int_A [\sigma_{xx}\epsilon_{xx} + \sigma_{zz}\epsilon_{zz} + \sigma_{yy}\epsilon_{yy} + \sigma_{xy}\epsilon_{xy} + \sigma_{xz}\epsilon_{xz} + \sigma_{yz}\epsilon_{yz}] dA dx + \int_0^l M_z' \kappa_z' dx. \tag{3}$$

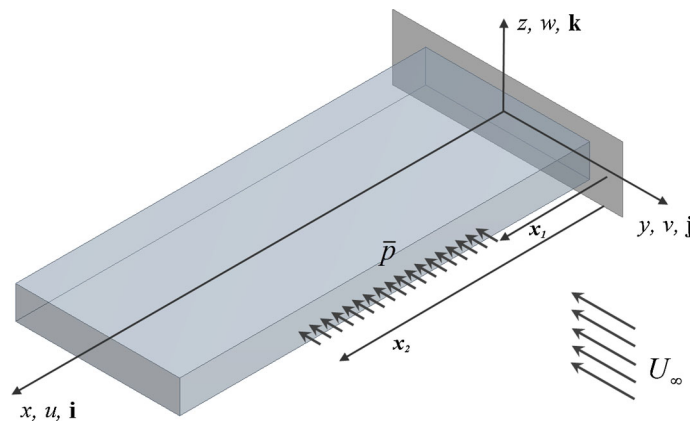


Fig. 1 A deep cantilever beam subjected to a partially distributed lateral force and a chord-wise flow

Assuming the deep cantilever beam to be long and slender, a uniaxial stress state can be imagined, i.e., $\sigma_x = \sigma_y = \sigma_z = 0$. Besides, the remaining stresses and strains can be expressed as follows [8]:

$$\begin{aligned} \sigma_{xx} &= E\varepsilon_{xx}, & \varepsilon_{xx} &= u' - yv'' - zw'', \\ \sigma_{xy} &= G\varepsilon_{xy}, & \varepsilon_{xy} &= -z\theta', \\ \sigma_{xz} &= G\varepsilon_{xz}, & \varepsilon_{xz} &= y\theta'. \end{aligned} \tag{4}$$

Moreover, the induced bending moment due to the laterally exerted follower force and the beam curvature in Eq. (3) can be presented as

$$\begin{aligned} M_{z'} &= \sum_i (-1)^{i+1} \frac{\bar{p}}{2} \{(x_i - x)^2 H(x_i - x)\}, \\ \kappa &= v'' + \theta w''. \end{aligned} \tag{5}$$

After some manipulations, assuming a linear equation of motion and ignoring terms of higher orders, the first variation of strain energy can be expressed as

$$\begin{aligned} \delta U &= \int_0^l \left\{ GJ\theta'\delta\theta' + \left(\sum_i (-1)^i \frac{\bar{p}}{2} \{(x_i - x)^2 H(x_i - x)\} \right) \delta v'' + EI_y w''\delta w'' \right. \\ &\quad \left. + \left(\sum_i (-1)^i \frac{\bar{p}}{2} \{(x_i - x)^2 H(x_i - x)\} \right) w''\delta\theta + \left(\sum_i (-1)^i \frac{\bar{p}}{2} \{(x_i - x)^2 H(x_i - x)\} \right) \theta\delta w'' \right\} dx. \end{aligned} \tag{6}$$

The virtual work done by the partially distributed follower force, δW_A and the induced lift and moment by free stream, δW_F in moving through virtual displacements is given by

$$\begin{aligned} \delta W &= \delta W_A + \delta W_F, \\ \delta W_A &= \bar{p} \int_0^l \left\{ \left(\sum_i (-1)^{i+1} H(x_i - x) \right) \mathbf{j}' \cdot [\delta u(x, t) \mathbf{i} + \delta v(x, t) \mathbf{j} + \delta w(x, t) \mathbf{k}] \right\} dx \\ &= \bar{p} \int_0^l \left\{ \left(\sum_i (-1)^{i+1} H(x_i - x) \right) (-v'\delta u + \delta v + \theta\delta w) \right\} dx, \\ \delta W_F &= \int_0^l (L\delta w + M\delta\theta) dx, \end{aligned} \tag{7}$$

where the lift and moment equations according to the Peters' finite state theory [17] and Qin and Librescu [18] are defined as:

$$\begin{aligned} L &= \pi\rho_\infty b^2 (-\ddot{w} + U_\infty\dot{\theta}) + C_{L\theta}\rho U_\infty b \left(-\dot{w} + U_\infty\theta + \frac{b}{2} \left(\frac{C_{L\theta}}{\pi} - 1 \right) \dot{\theta} - \lambda_0 \right), \\ M &= -\pi\rho_\infty b^3 \left(\frac{1}{2} \left(\frac{C_{L\theta}}{\pi} - 1 \right) U_\infty\dot{\theta} + \frac{b}{8}\ddot{\theta} \right) - \frac{1}{2} C_{L\theta}\rho_\infty U_\infty b^2 \left(\dot{w} - U_\infty\theta - \frac{b}{2} \left(\frac{C_{L\theta}}{\pi} - 1 \right) \dot{\theta} - \lambda_0 \right), \end{aligned} \tag{8}$$

where $C_{L\theta}$ can be found in [19]. Also, the induced flow velocity in terms of cross section motion in accordance with Peters' theory can be expressed as

$$\lambda_0 \approx \frac{1}{2} \sum_1^N b_n \lambda_n. \tag{9}$$

Herein, the induced flow velocities, $\lambda_1, \dots, \lambda_N$, are obtained by solving the following first-order differential equations:

$$[\mathbf{A}] \{\dot{\lambda}\} + \frac{U_\infty}{b} \{\lambda\} = \{\mathbf{c}\} \left[-\dot{w} + U_\infty \dot{\theta} + \frac{b}{2} \left(\frac{C_{L\theta}}{\pi} - 1 \right) \ddot{\theta} \right], \tag{10}$$

where the matrix $[\mathbf{A}]$ and vectors $\{\mathbf{b}\}$ and $\{\mathbf{c}\}$ can be found in [17]. For the case of a deep cantilever beam subjected to a partially distributed lateral follower force, the following boundary conditions are applicable:

$$v(0) = v'(0) = w(0) = w'(0) = \theta(0) = 0. \tag{11}$$

Substituting the above work and energy terms in Eq. (1) and integrating by parts, results in the weak form of the equation of motion. Applying the above boundary conditions and collecting the coefficients of δw and $\delta \theta$, the torsional-flexural equation of motion of a deep cantilever beam subjected to a lateral follower force with partial distribution when exposed to a chord-wise flow can be presented as

$$\begin{aligned} & \rho A \ddot{w} + \rho A c \ddot{\theta} + EI_{y'} w'''' - C_{L\theta} \rho_\infty U_\infty b \left(-\dot{w} + U_\infty \dot{\theta} + \frac{b}{2} \left(\frac{C_{L\theta}}{\pi} - 1 \right) \dot{\theta} - \lambda_0 \right) \\ & - \pi \rho_\infty b^2 (-\ddot{w} + U_\infty \dot{\theta}) + \sum_i (-1)^{i+1} \bar{p} \left[\left[\frac{1}{2} (x_i - x)^2 H(x_i - x) \right] \theta'' \right. \\ & \left. - [2(x_i - x) H(x_i - x)] \theta' \right] = 0, \\ & \rho A k_m^2 \ddot{\theta} + \rho A c \ddot{w} - G J \theta'' + \left(\sum_i (-1)^{i+1} \left[\frac{1}{2} \bar{p} (x_i - x)^2 H(x_i - x) \right] \right) w'' \\ & + \pi \rho_\infty b^3 \left(\frac{1}{2} \left(\frac{C_{L\theta}}{\pi} - 1 \right) U_\infty \dot{\theta} + \frac{b}{8} \ddot{\theta} \right) \\ & + \frac{1}{2} C_{L\theta} \rho_\infty U_\infty b^2 \left(\dot{w} - U_\infty \dot{\theta} - \frac{b}{2} \left(\frac{C_{L\theta}}{\pi} - 1 \right) \dot{\theta} + \lambda_0 \right) = 0. \end{aligned} \tag{12}$$

2.3 Stability methodology

Due to the intricacy of the coupled structural and aerodynamic governing equations, the solution of this problem is sought among the approximate solution methods. Here, the Galerkin approach is utilized with two distinct approximation functions, one for bending and the other for torsional dynamics:

$$w(x, t) = \boldsymbol{\Phi}^T(x) \boldsymbol{\xi}_w(t), \quad \theta(x, t) = \boldsymbol{\Psi}^T(x) \boldsymbol{\xi}_\theta(t), \tag{13}$$

in which $\boldsymbol{\xi}_w(t)$ and $\boldsymbol{\xi}_\theta(t)$ are time-dependent vectors of the generalized coordinates. Besides, $\boldsymbol{\Phi}$ and $\boldsymbol{\Psi}$ are the free vibration natural modes of bending and torsion, respectively, which satisfy the boundary conditions as shown below [20]:

$$\phi_i(x) = \cosh(\alpha_i x) - \cos(\alpha_i x) - \beta_i [\sinh(\alpha_i x) - \sin(\alpha_i x)], \quad \cosh(\alpha_i L) \cos(\alpha_i L) + 1 = 0, \tag{14}$$

$$\psi_i(x) = \sin(\gamma_i x), \quad \gamma_i = \frac{(2i - 1)\pi}{2L}. \tag{15}$$

Discretizing the governing equations using the Galerkin procedure, a set of second-order differential equations of motion is obtained. Defining the state variables $Z = \{\boldsymbol{\xi}_w, \boldsymbol{\xi}_\theta, \dot{\boldsymbol{\xi}}_w, \dot{\boldsymbol{\xi}}_\theta, \boldsymbol{\lambda}\}^T$, the second-order differential equations can be transformed into the first-order state space representation of the governing equations:

$$\{\dot{\mathbf{Z}}\} = [\mathbf{A}] \{\mathbf{Z}\}. \tag{16}$$

As a result of the non-conservative nature of system, the eigenproblem of Eq. (16) is non-self-adjoint and hence the eigenvalues of the state matrix, $[\mathbf{A}]$, are generally complex quantities, i.e., $\omega = \text{Re}(\omega) + i \text{Im}(\omega)$. The stability and instability regions and type of instability can be analyzed based on the sign and magnitude of the real and imaginary parts of the eigenvalues [21].

3 Numerical results and discussions

In order to verify the accuracy of the proposed model, the results of the simulations are compared for the case of fully distributed follower force when the effect of free stream is disregarded. Figure 2 shows that a good agreement exists between the current modeling and the results of Fazelzadeh and Kazemi-Lari [15], for the variations of frequency versus the follower force. It should be noted that more modes (six modes for bending and six modes for torsion) are used in the present study to improve the accuracy, in comparison with [15] which used four modes. Also, for simplicity of numerical simulations, the following dimensionless parameters are introduced:

$$\begin{aligned}
 X &= \frac{x}{l}, & \bar{c} &= \frac{c}{l}, & \sigma &= \frac{k_m}{l}, & v_\infty &= \frac{U_\infty}{b\omega_\theta}, \\
 \tau &= \frac{t}{l^2} \sqrt{\frac{EI_{y'}}{\rho A}}, & \bar{P} &= \frac{\bar{p}l^3}{\sigma EI_{y'}}, & r^2 &= \frac{EI_{y'}\sigma^2 \alpha_1^4}{GJ \gamma_1^2}.
 \end{aligned}
 \tag{17}$$

Herein, r is the ratio of fundamental bending and torsion frequencies of the unloaded beam with $c = 0$.

3.1 Eigenvalue analysis

In this section, variations of the imaginary parts of the eigenvalues or frequency of vibrations and the real parts of the eigenvalues, or the amplitude decaying rate, for different locations of the follower force along the beam's span are examined. The effect of the free stream is ignored, and the force distribution length is assumed to be $0.25l$. As it is seen in Fig. 3a, for $r = 3/2$, the first bending and torsion modes coalesce around $\bar{P} = 11.75, 23.25, 82.50$ for $0.75 \leq X_i \leq 1.00, 0.50 \leq X_i \leq 0.75,$ and $0.25 \leq X_i \leq 0.50$, respectively, with the corresponding flutter frequency of $\text{Im}(\omega) = 2.88, 2.90,$ and 2.97 . As it is observed, the force distribution location remarkably affects the dynamic instability load but the flutter frequencies are nearly identical for these cases. Moreover, the beam undergoes a divergence instability type for $\bar{P} = 94.25$ when $0.75 \leq X_i \leq 1.00$. Variations of the real parts of the eigenvalues are depicted in Fig. 3b. A bifurcation in values is observed at the critical forces. Also, a second bifurcation happens for $0.75 \leq X_i \leq 1.00$ corresponding to divergence instability load.

3.2 Force distribution models

The cantilever beam might be subjected to the distributed follower force in different configurations. Table 1 shows the proposed models for load distribution. For all these four patterns, the stability boundaries are derived

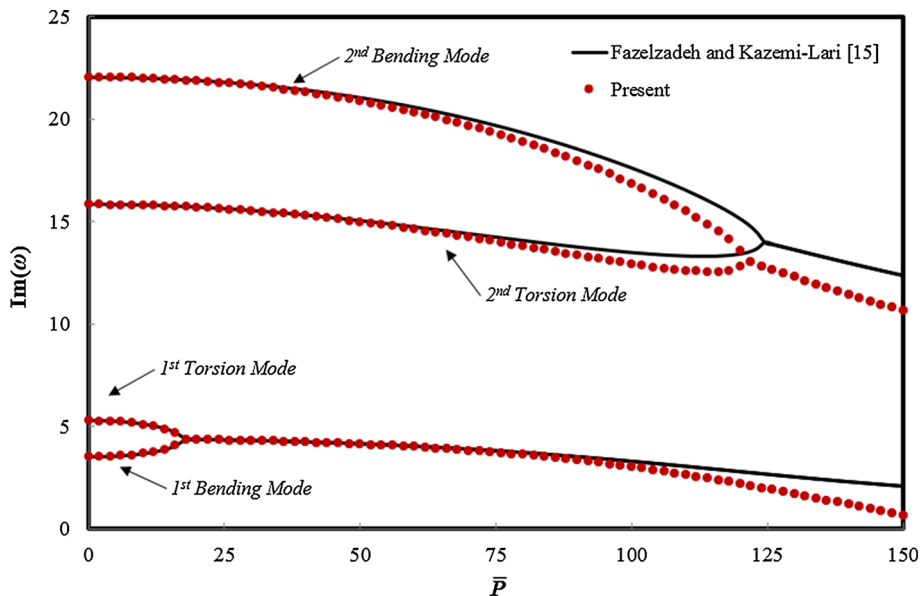


Fig. 2 Model validation against the results of Fazelzadeh and Kazemi-Lari [15] for $r = 2/3$ and $\bar{c} = 0.000$

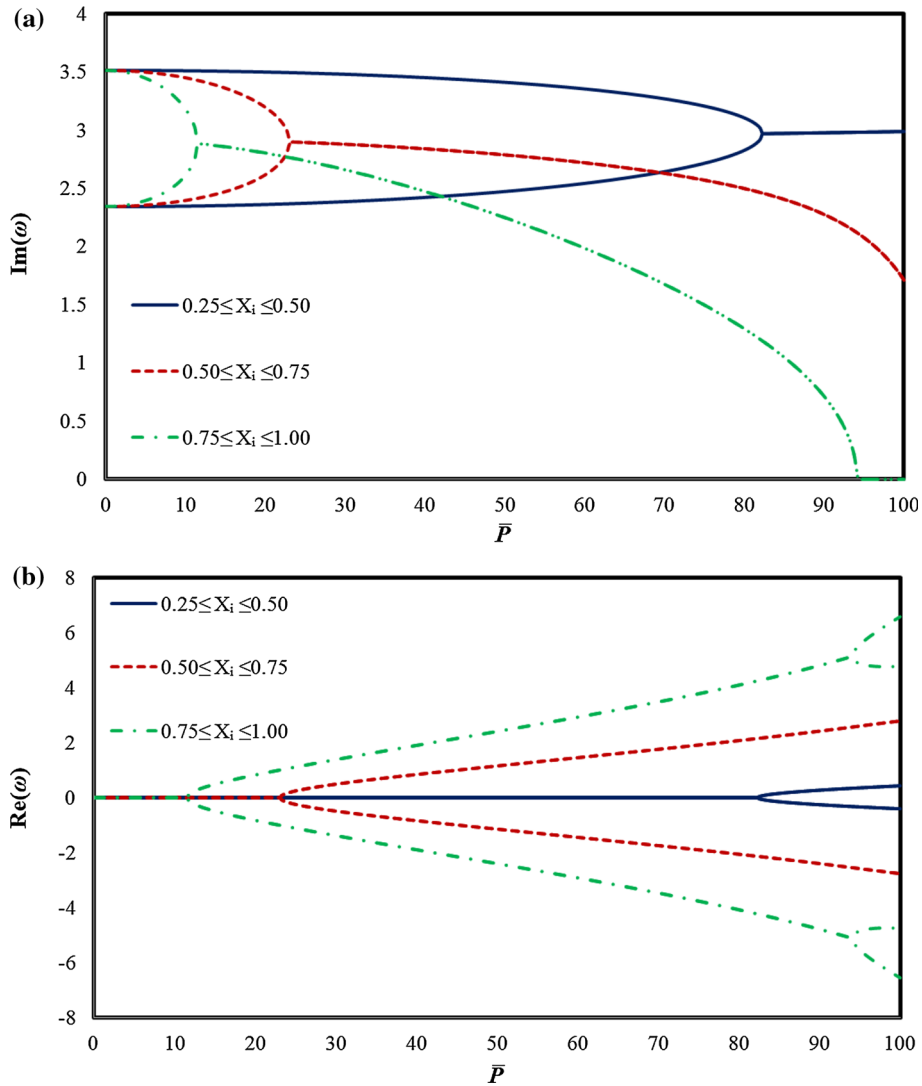


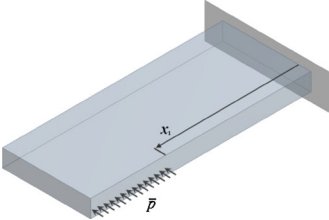
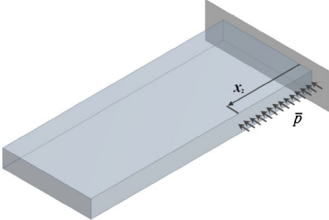
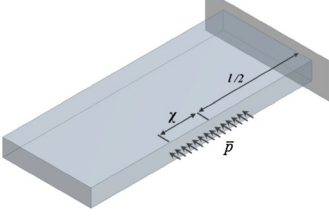
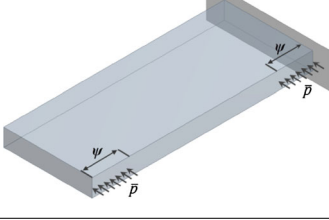
Fig. 3 Variations of **a** imaginary and **b** real parts of the eigenvalues versus \bar{P} for different loading conditions

with respect to changes in follower force magnitude and for different fundamental frequencies ratios, mass centroid offsets, and radii of gyration.

Figure 4a demonstrates the variations of the critical follower force for different values for the fundamental frequencies ratio, $r = 0.6, 1.4, \text{ and } 2.0$. For this analysis, it is assumed that the mass centroid is coincident with the elastic axis. According to this figure, up to $X_1 = 0.375$, the flutter force is approximately constant for all these values. As X_1 increases, i.e., the length of the force distribution decreases, the critical follower force increases. This increase is much more considerable for $r < 1$. Figure 4b displays the variations for different values of mass centroid offset, $\bar{c} = -0.005, 0.000, \text{ and } 0.005$ assuming $r = 2/3$ and $\sigma = 0.025$. It is observed that as the mass centroid is further displaced in the $+y$ direction, the critical force decreases. For this case again, the critical force is approximately unvarying up to $X_1 = 0.375$. The stability boundary for different values of non-dimensionalized radius of gyration, $\sigma = 0.005, 0.010, \text{ and } 0.020$, is depicted in Fig. 4c with $r = 2/3$ and $\bar{c} = 0.005$. As the radius of gyration increases, i.e., increase in mass distribution relative to the elastic axis, the critical load decreases. Also, for all values of σ , the critical force increase for $X_1 > 0.375$ and this increase is much more noticeable for smaller radius of gyration.

Figure 5 presents the flutter boundary for the second force distribution model. It can be seen again that the flutter boundary is much higher for smaller values of r and σ . Also, it can be found from Fig. 5b that the

Table 1 Different types of load distribution models

	Distribution model	Description
Model 1		$X_2 = 1$ and $0.000 < X_1 < 0.750$
Model 2		$X_1 = 0$ and $0.500 < X_2 < 1.000$
Model 3		$0.125 < \chi < 0.500$
Model 4		$0.125 < \psi < 0.500$

negative values of mass centroid offset have a considerable influence on the critical load, while the positive values of \bar{c} causes a slight decrease in the flutter load when compared to $\bar{c} = 0.000$.

Variations of the critical force with respect to the changes in load distribution length of model 3 are plotted in Fig. 6. In this model, the load distribution length increases from the mid-span toward the ends. As it is indicated, the stability region extenuates as the distribution length increases and this reduction is much more significant for $\chi < 0.3125$.

Finally in Fig. 7, the stability boundary is plotted versus the load increment of model 4. In this model, the cantilever beam is subjected to the lateral force in two segments. In this case, again the flutter force monotonically declines as the total length of the force increases and this decrease is more considerable for $\psi < 0.3125$.

From the above results, it can be inferred that for the same load distribution length and physical parameters, the magnitude of the critical force can be sorted by model 2 > model 3 > model 4 > model 1.

3.3 Free stream effect

In this section, the influence of a free stream with chord-wise flow velocity is considered on the dynamic instability of the deep cantilever. The flutter boundary for different load distribution models has been plotted with respect to changes in non-dimensionalized flow velocity, v_∞ . In order to draw a better comparison between

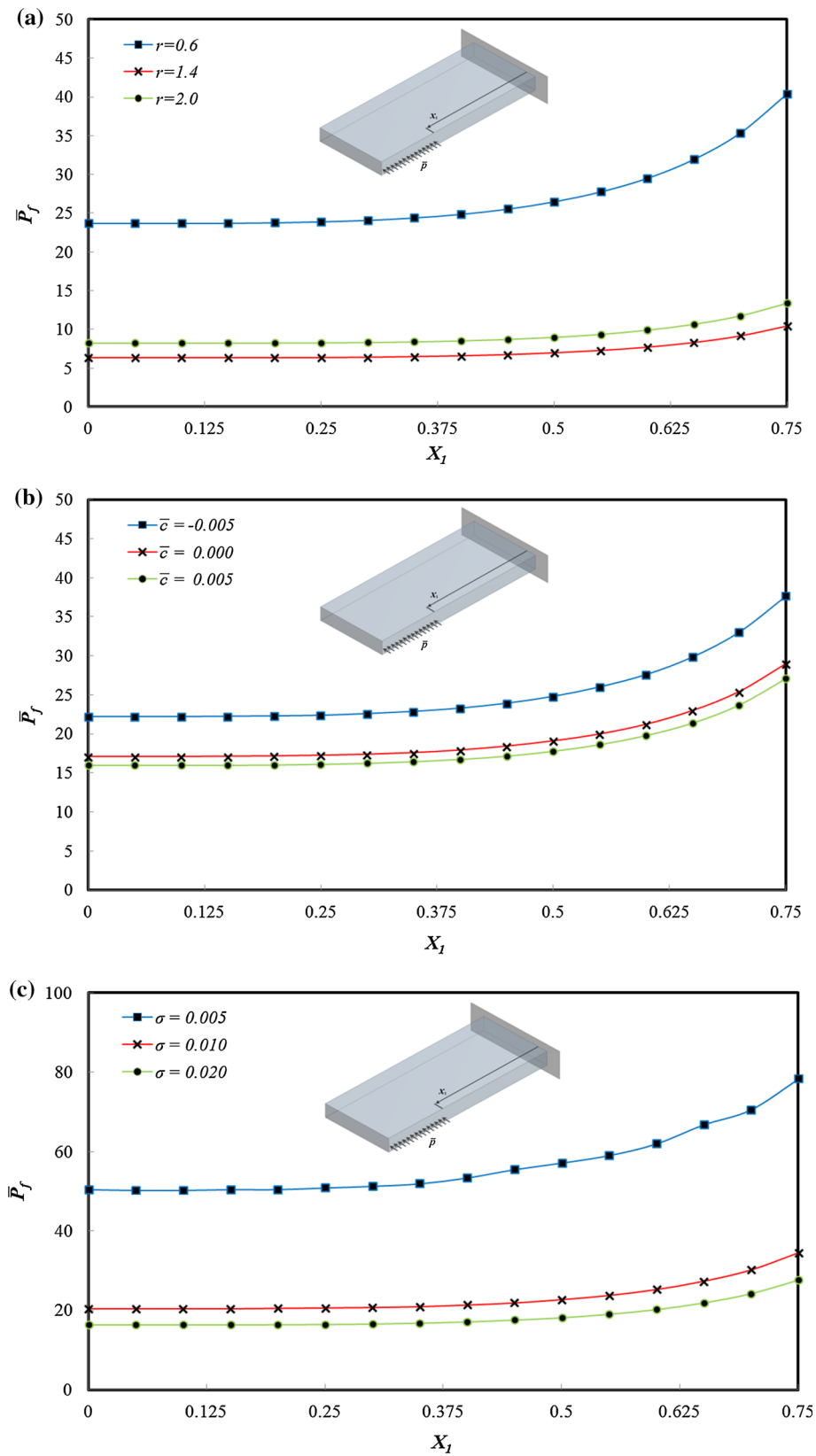


Fig. 4 Flutter boundary versus load distribution length increment of model 1 for different values of **a** r , **b** σ , and **c** \bar{c}

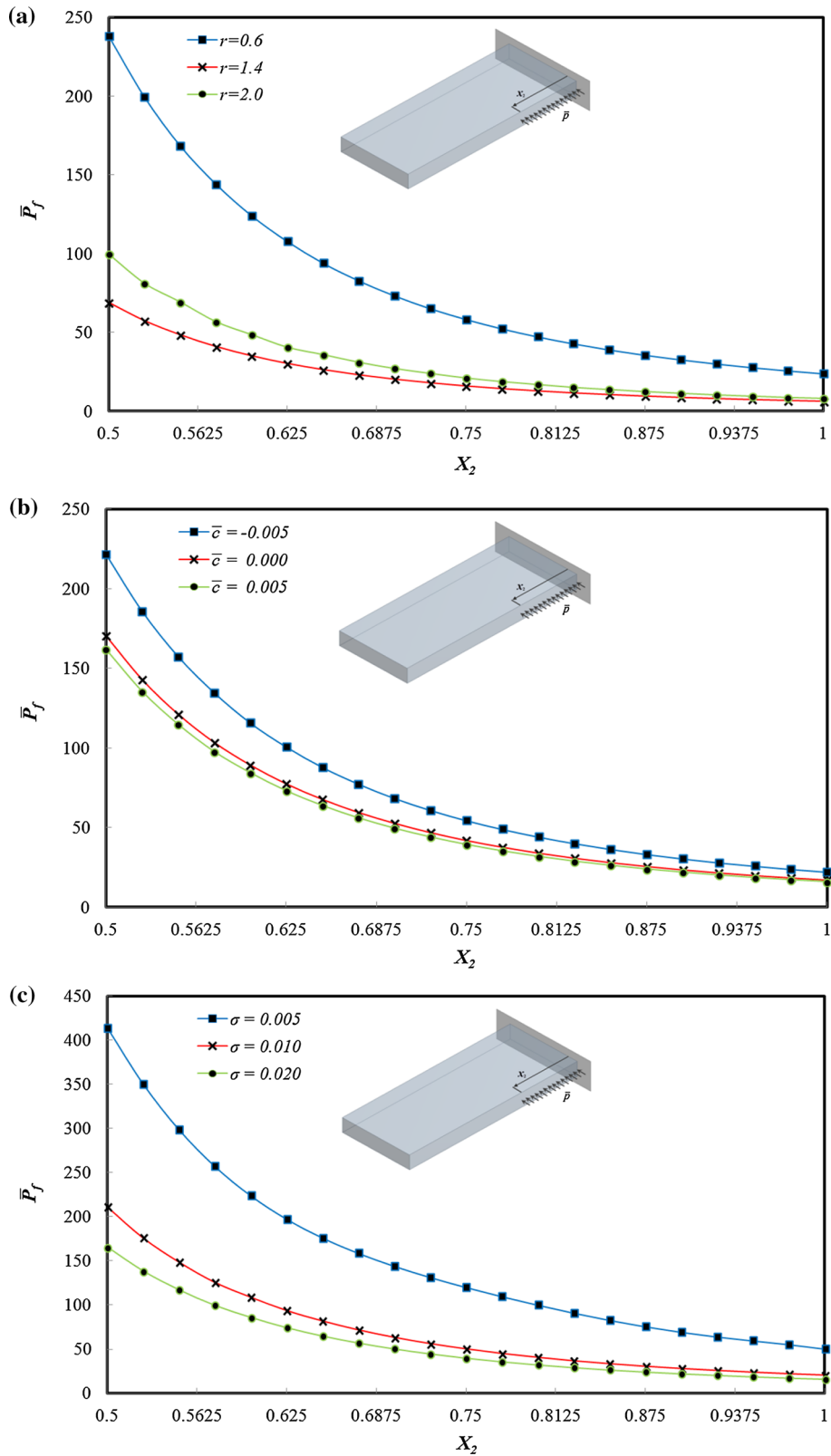


Fig. 5 Flutter boundary versus load distribution length increment of model 2 for different values of a , b , σ , and \bar{c}

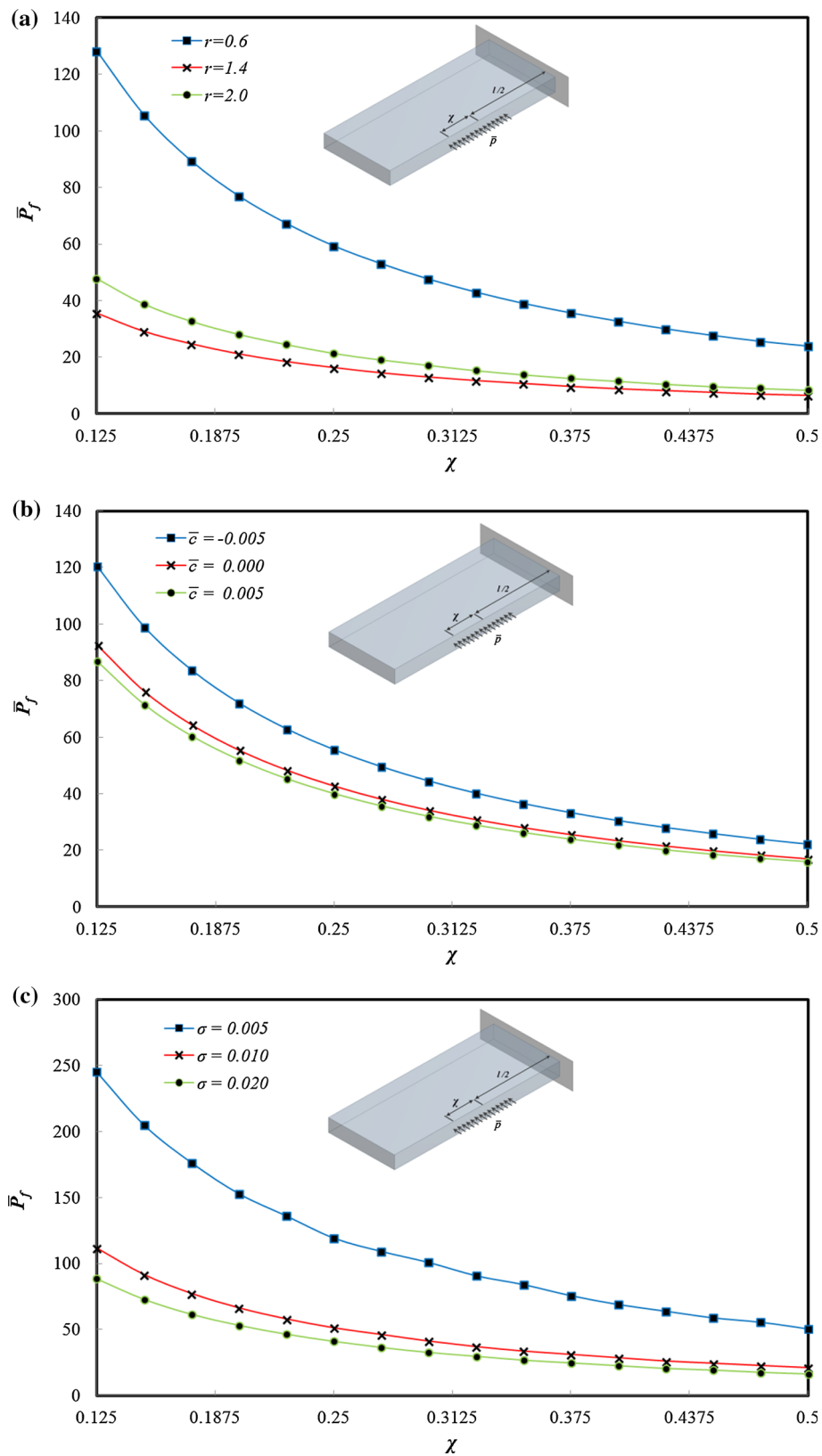


Fig. 6 Flutter boundary versus load distribution length increment of model 3 for different values of a r , b σ , and c \bar{c}

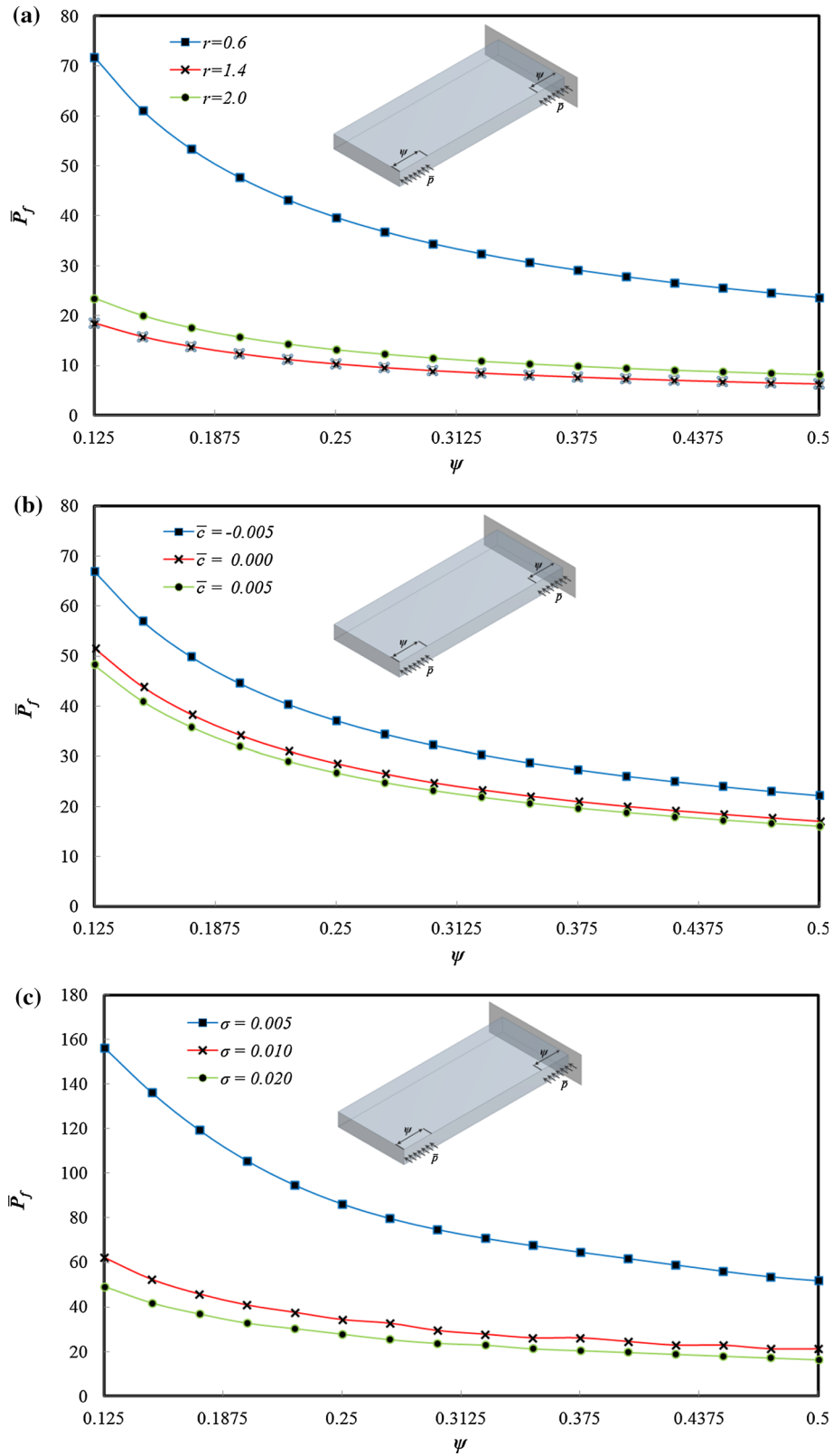


Fig. 7 Flutter boundary versus load distribution length increment of model 4 for different values of a , r , b , σ , and c

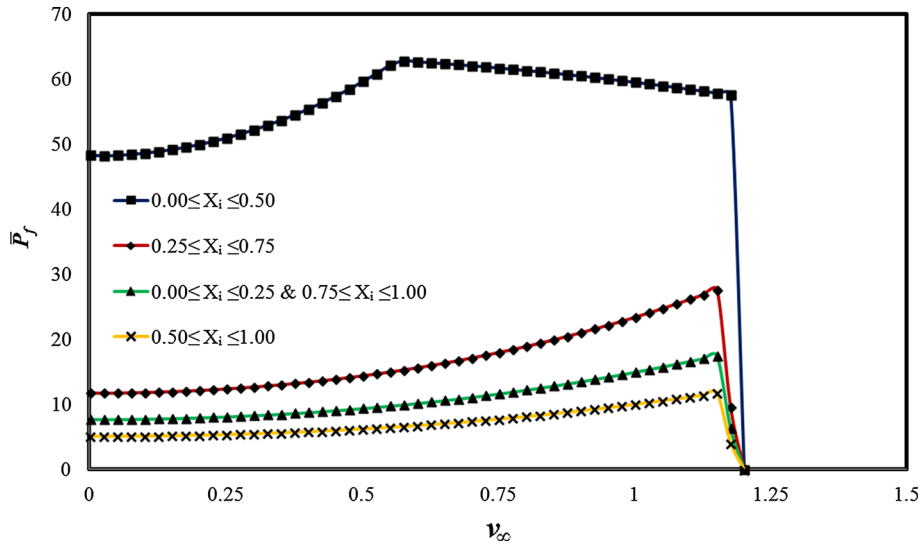


Fig. 8 Variations of the critical load with respect to free stream velocity increment for different load distribution conditions

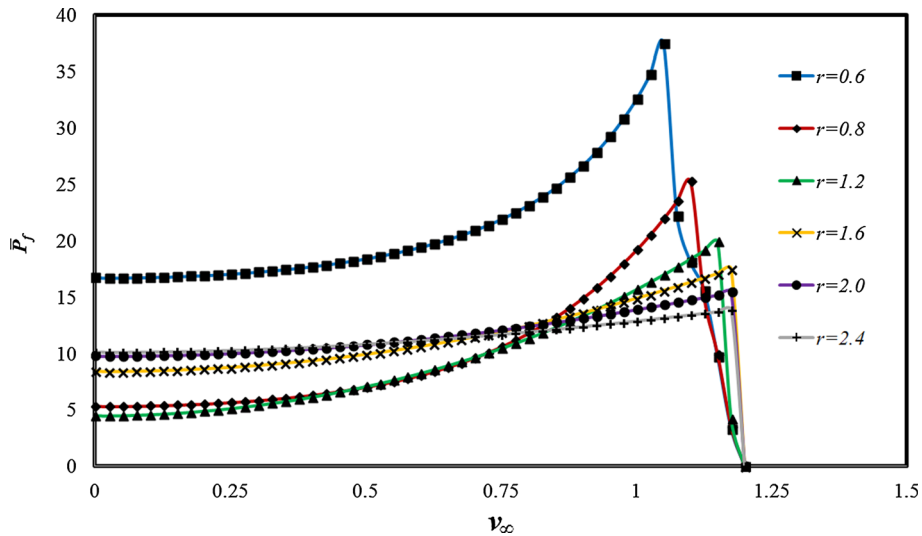


Fig. 9 Variations of the critical load with respect to free stream velocity increment for various values of r

the loading conditions, the total length of the follower force is assumed to be $0.5l$ for all the models. The values of other parameters are set to be $r = 3/2$ and $\bar{c} = 0.000$. According to Fig. 8, the stable region is much greater when the load is applied in the first half of the beam span near the root. This is because the beam obtains less-positive work from the distributed force when compared with other models. Moreover, the flutter boundary for all models converges at $v_\infty = 1.2$, in which the beam flutters merely due to the free stream velocity.

Figure 9 represents the variations of the critical load versus the increase in free stream velocity for different frequency ratios and $\bar{c} = 0.000$. It is seen that for all values of r , the required force for dynamic instability rises uniformly as the free stream velocity increases. The critical load reaches a maximum value and then suddenly declines as the flow velocity increases. It is observed that this maximum value is greater for smaller frequency ratios but the flutter boundaries come together at $v_\infty = 1.2$ for all values of r .

Changes in the flutter boundary versus the free stream velocity for different values of non-dimensionalized mass centroid offset are shown in Fig. 10. It can be found that the stable region gets smaller as the mass centroid is moved toward the $+y$ direction. Moreover, it is shown again that increasing the free stream velocity has a stabilizing effect up to some certain values and has a destabilizing effect after that.

Increasing the radius of gyration is shown to have two distinct influences on the beam's vibration as shown in Fig. 11. First, it can be inferred that as the radius of gyration is increased, the critical load decreases regardless

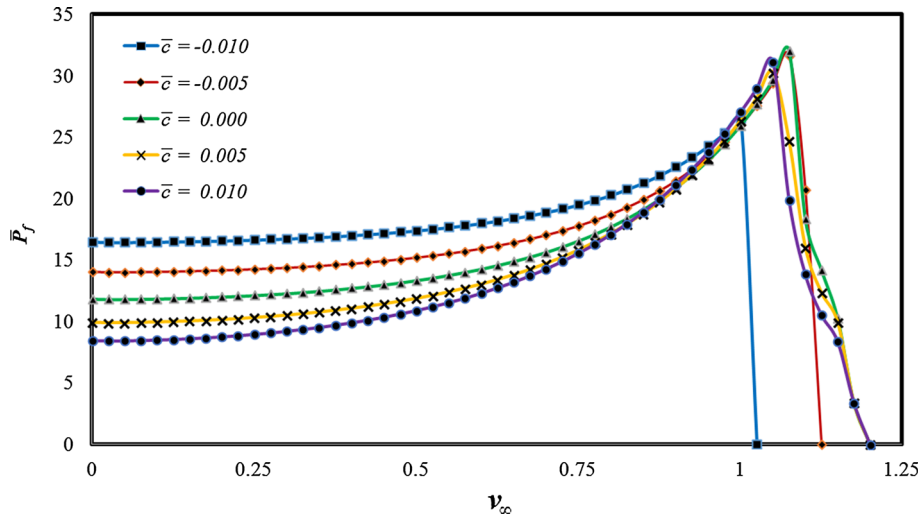


Fig. 10 Variations of the critical load with respect to free stream velocity increment for various values of \bar{c}

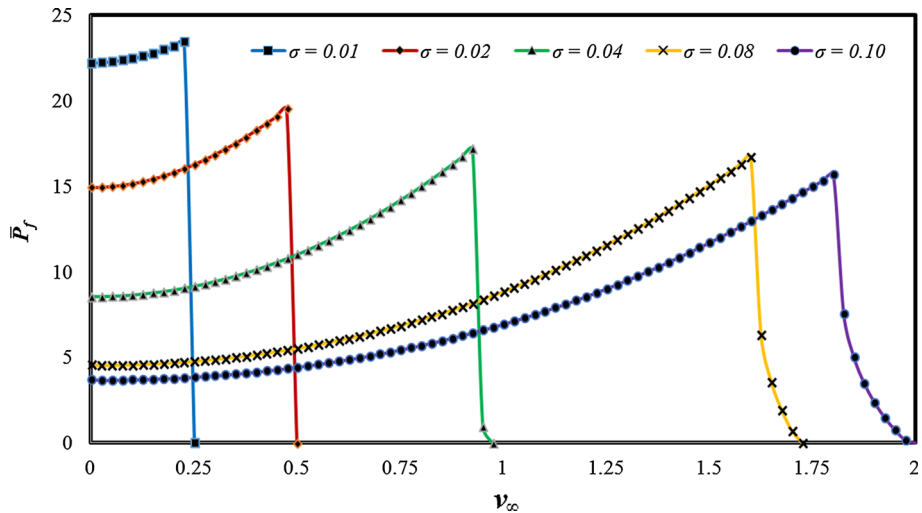


Fig. 11 Variations of the critical load with respect to free stream velocity increment for various values of σ

of the free stream velocity. In addition, the stable region is shown to have a greater area for smaller radii of gyration as the velocity increases. Also, the critical flow velocity, for which the beam flutters regardless of the magnitude of the follower force, increases as the radius of gyration increases.

4 Conclusion

The coupled torsional-flexural instability analysis of deep cantilever beams considering the influence of a partially distributed lateral force and free stream was investigated. Considering a partial distribution for the lateral follower force was the main contribution of the present study. It was demonstrated that the force distribution location remarkably affects the critical load but the flutter frequencies were nearly identical for the different load distribution models. Besides, the flutter boundary was examined for these load distribution models and system parameters like the ratio of flexural to torsional rigidities, radius of gyration, and mass centroid offset. It was shown that for all models, the critical load increases when the mass centroid is moved toward the $-y$ direction and slightly decreases when moved in the $+y$ direction. Also it was indicated that the stable region shrinks when the radius of gyration is increased. Moreover, it was found that the required

force for dynamic instability condition reaches its minimum value when the fundamental frequency ratio tends toward unity.

The free stream was indicated to have a stabilizing effect on the beam's vibration up to some specified values. Further increase in the free stream velocity was shown to cause an abrupt decrease in the flutter load. It was also observed that the flutter boundaries for all load distribution models and the selected values of r converge at a critical flow velocity in which the dynamic instability takes place regardless of the applied force. Moreover, it was found that the stable region got smaller as the mass centroid moved toward the $+y$ direction. Furthermore, it was demonstrated that the flutter boundary was much higher and the stable region was much smaller for smaller values of radius of gyration as the free stream velocity increased.

References

1. Beck, M.: Die Knicklast des einseitig eingespannten, tangential gedrückten Stabes [The buckling load of the cantilevered, tangentially compressed rod]. *ZAMP* **3**, 225–228 (1952)
2. Como, M.: Lateral buckling of a cantilever subjected to a transverse follower force. *Int. J. Solids Struct.* **2**, 515–523 (1966)
3. Ziegler, H.: *Principles of Structural Stability*. Blaisdell, Waltham (1968)
4. Leipholz, H.: Die Knicklast des einseitig eingespannten Stabes mit gleichmässig verteilter, tangentialer Längsbelastung [The buckling load of the cantilevered rod with uniformly distributed, tangential longitudinal stress]. *ZAMP* **13**, 581–589 (1962)
5. Bolotin, V.V.: *Non-conservative Problems of Theory of Elastic Stability*. Pergamon Press, Oxford (1963)
6. Simitses, G.J., Hodges, D.H.: *Fundamentals of Structural Stability*. Elsevier, Burlington (2006)
7. Langthjem, M.A., Sugiyama, Y.: Dynamic stability of columns subjected to follower loads: a survey. *J. Sound Vib.* **238**, 809–851 (2000)
8. Hodges, D.H.: Lateral-torsional flutter of a deep cantilever loaded by a lateral follower force at the tip. *J. Sound Vib.* **247**, 175–183 (2001)
9. Fazelzadeh, S.A., Mazidi, A., Kalantari, H.: Bending-torsional flutter of wings with an attached mass subjected to a follower force. *J. Sound Vib.* **323**, 148–162 (2009)
10. Feldt, W.T., Herrmann, G.: Bending-torsional flutter of a cantilevered wing containing a tip mass and subjected to a transverse follower force. *J. Frankl. I.* **297**, 467–478 (1974)
11. Hodges, D.H., Patil, M.J., Chae, S.: Effect of thrust on bending-torsion flutter of wings. *J. Aircr.* **39**, 371–376 (2002)
12. Mazidi, A., Kalantari, H., Fazelzadeh, S.A.: Aeroelastic response of an aircraft wing with mounted engine subjected to time-dependent thrust. *J. Fluids Struct.* **39**, 292–305 (2013)
13. Mardanpour, P., Richards, P.W., Nabipour, O., Hodges, D.H.: Effect of multiple engine placement on aeroelastic trim and stability of flying wing aircraft. *J. Fluids Struct.* **44**, 67–86 (2013)
14. Fazelzadeh, S.A., Kazemi-Lari, M.A.: Stability analysis of partially loaded Leipholz column carrying a lumped mass and resting on elastic foundation. *J. Sound Vib.* **332**, 595–607 (2013)
15. Fazelzadeh, S.A., Kazemi-Lari, M.A.: Stability analysis of a deep cantilever beam with laterally distributed follower force. *J. Eng. Mech. ASCE* **140**(10), 04014074 (2014)
16. Anderson, G.L.: The influence of rotatory inertia, tip mass, and damping on the stability of a cantilever beam on an elastic foundation. *J. Sound Vib.* **43**, 543–552 (1975)
17. Peters, D.A., Karunamoorthy, S., Cao, W.M.: Finite state induced flow models. Part I: Two-dimensional thin airfoil. *J. Aircr.* **32**, 313–322 (1995)
18. Qin, Z., Librescu, L.: Aeroelastic instability of aircraft wings modelled as anisotropic composite thin-walled beams in incompressible flow. *J. Fluids Struct.* **18**, 43–61 (2003)
19. Bisplinghoff, R.L., Ashley, H., Halfman, R.L.: *Aeroelasticity*. Addison Wesley, Cambridge (1955)
20. Fletcher, C.A.J.: *Computational Galerkin Methods*. Springer, New York (1984)
21. Seyranian, A.P., Mailybaev, A.A.: *Multiparameter Stability Theory with Mechanical Applications*. World Scientific, Singapore (2003)